

## MESO-SCALE MODELING FOR FIBER REINFORCED CONCRETE UNDER MIXED MODE FRACTURE

HIROKI OGURA<sup>\*</sup>, MINORU KUNIEDA<sup>†</sup>, NAOSHI UEDA<sup>†</sup> AND HIKARU NAKAMURA<sup>†</sup>

<sup>\*</sup> Shimizu Corporation, Institute of Technology  
Tokyo, JAPAN  
e-mail: ogura\_h@shimz.co.jp

<sup>†</sup> Nagoya University, Dept. of Civil Engineering  
Nagoya, JAPAN  
e-mail: kunieda@nagoya-u.jp (M. Kunieda)

**Key words:** Fiber Reinforced Concrete, Meso-scale Analysis, Rigid-Body-Spring Model (RBSM)

**Abstract:** This paper introduces the meso-scale modeling of fiber reinforced concrete under mixed mode fracture. Fibers and matrix are modeled separately in this model, and each fiber is randomly arranged within the specimen models. The feature of this analytical model is to evaluate fiber resistance against shear deformation across the crack plane by calculating the pullout angle and the pullout displacement of each fiber. In order to validate the modeling, fracture analysis of the specimen with punching shear failure was conducted. It was confirmed that the proposed model can roughly simulate the failure of fiber reinforced concrete including crack patterns and load carrying capacity.

### 1 INTRODUCTION

There are a wide variety of short fiber reinforced cement composites. One of the materials is Strain Hardening Cementitious Composites (SHCC) that exhibit strain hardening and multiple cracking in tension. Quantitative material design methods considering the properties of matrix, fiber and their interface should be established. In addition, numerical models to simulate the fracture process including crack width and crack distribution for the material are needed.

Bolander & Saito [1], for instance, conducted 2-D parametric analysis in which short fibers were discretized as beam elements to examine the effect of the fiber distribution on the mechanical performance of the resulting composite. The authors also have proposed a numerical model for 3-D analysis of SHCC

tensile fracture, in which the salient features of the material meso-scale (i.e. matrix, fibers and their interface) are discretized [2-3]. This model has the following characteristics: (1) the fibers with a specific length are randomly arranged as discrete entities within the specimen models; (2) crack patterns can be estimated in addition to the improvement of mechanical responses due to fiber bridging. It has been confirmed that the proposed model can adequately simulate the tensile failure of SHCC including crack patterns [2].

This paper proposes an advanced model, which can simulate the failure of fiber reinforced concrete under mixed mode fracture, in order to expand scope of the aforementioned analysis. The feature of the advanced model is to evaluate fiber resistance against shear deformation across the crack plane by calculating the pullout angle and the pullout displace-

ment of each fiber. In order to validate the modeling, fiber pullout analysis and fracture analysis of the specimen with punching shear failure was conducted.

## 2 OUTLINE OF RBSM

In this study, the concrete matrix (hereinafter, matrix) is represented by 3-D RBSM. Figure 1 shows an example of a pair of Voronoi cells composing the element stiffness matrix in the RBSM. These Voronoi cells are assumed to be rigid bodies, while setting 6 degrees of freedom for each rigid Voronoi cell. 6 springs are placed on each boundary plane of each cell, in the normal (1 spring) and tangential (2 springs) to the boundaries and rotational directions (3 springs).

The material properties (tensile strength, elastic modulus, and fracture energy) of the matrix are adopted as the mechanical properties of the normal and tangential springs, whereas the mechanical properties of the rotational springs are assumed based on the literature [4]. As the tensile model of normal spring, linear elastic model is employed up to tensile strength, and a bilinear softening branch in accordance with a 1/4 model is considered after cracking. Tensile fracture energy is taken into consideration in the model. For tangential springs, the Mohr-Coulomb fracture criterion is applied to represent the shearing behavior of concrete [5].

When using a RBSM, the onset and propagation of cracks are strongly affected by the mesh size and shape. Therefore, such dependence is minimized by adopting Voronoi discretization based on randomly placed seed points.

## 3 MODELLING OF FIBER ACTION AFTER CRACKING

### 3.1 Conventional model

Short fibers of a specified length are arranged in elements assuming the specimen size to be analyzed, as shown in Figure 2 (a). Random numbers are used for the arrangement to decide first vertex and fiber angle. As

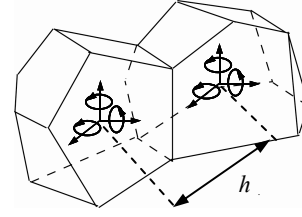


Figure 1: Voronoi cells and defined freedom degree.

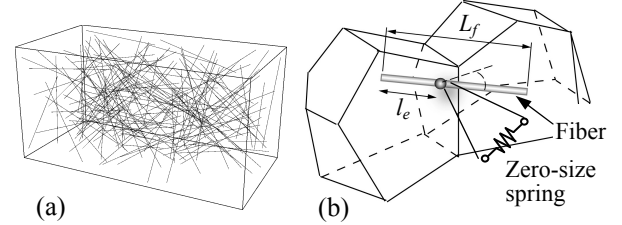


Figure 2: (a) Discretized fiber; (b) Fiber location and zero-size spring.

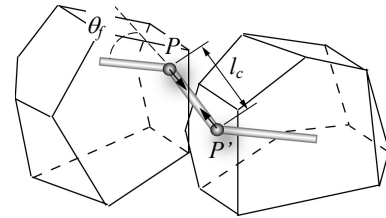


Figure 3: Modeling fiber bridging force against shear deformation.

shown in Figure 2(b), a zero-size spring is placed on a point where a fiber crosses a boundary of two Voronoi cells, and the force transfer by fibers across a crack plane (hereinafter, fiber bridging force) acted on the spring. The embedment length  $l_e$  is also calculated for each fiber. Note that, a shorter embedment length is defined as  $l_e$ . It is assumed that pullout behavior of the fiber prevails at a shorter side of the embedment length.

In a conventional model, the crack width of the matrix is used in order to assume the fiber pullout displacement, and the fiber bridging force is calculated by considering the pullout displacement and bond characteristic of the fiber [2]. This is a model which only considers the pullout behavior of the fiber in normal direction against crack plane. In short, normal force to the crack plane due to crack opening is modeled, but the fibers do not contribute to resistance produced by shear deformation perpendicular to crack opening.

### 3.2 Advanced model

A model based on a pullout behavior including the pullout angle of fibers, is proposed as an advanced model, in order to consider the fiber resistance against shear deformation across the crack plane. One of the improvements is to calculate the fiber length between the crack plane  $l_c$  shown in Figure 3.  $l_c$  is used instead of crack width to assume the length of fiber pullout displacement. With this method, fiber resistance can be analyzed, even if only shear deformation are excessive without crack opening. In addition, the pullout angle  $\theta_f$  of each fiber is calculated in each analytical step to consider the change in  $\theta_f$  depending on the direction of the shear deformation.  $\theta_f$  is calculated from  $P$  and  $P'$  (Figure 3), where  $P$  and  $P'$  are points where a fiber crosses a boundary of two cells after deformation.

In the advanced model, the fiber bridging force is calculated by the steps shown in Figure 4. Half of  $l_c$  is assumed to be the length of fiber pullout displacement before softening of fiber bridging force-displacement relation. After softening, pullout displacement is assumed to be equal to  $l_c$ . The shape of slip distribution is determined through the analysis of single fiber pullout tests. If the shape of slip distribution is known, then the bond stress distribution is determined from the bond stress-slip relation. The fiber bridging forces across cracks can then be calculated by integrating the bond stress distribution in the direction of the fiber axis.

At this stage, the slip distribution of a fiber and the bond stress-slip relation are necessary. These are identified in the same manner as the existing method [3], by conducting analysis of single fiber pullout bond testing [6] as stated in the following chapter.

### 3.3 Effect of the pullout angle

Li et al. [7] revealed the increase of pullout resistance in the inclined fiber pullout test. It has also been experimentally confirmed that the strength of inclined fiber itself was decreased due to surface damage during the pullout process. Therefore, in this study, the

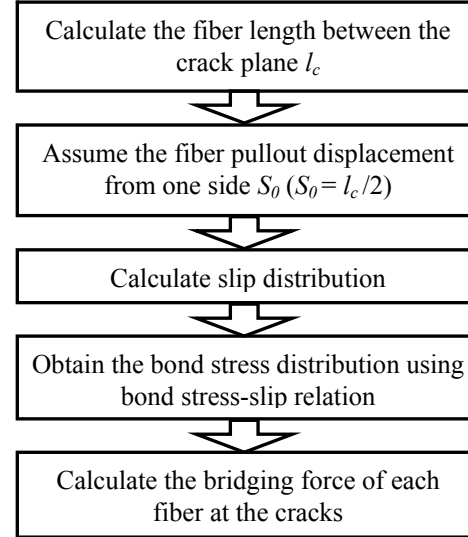


**Figure 4:** Procedure for calculation of fiber bridging force.

effect of the pullout angle  $\theta_f$  is calculated using the following equations [7]:

$$F = F^n e^{f \theta_f} \quad (\theta_f \leq 45^\circ) \quad (1)$$

$$\sigma_{fu} = \sigma_{fu}^n e^{f' \theta_f} \quad (2)$$

where  $F$  = pullout load (N),  $F^n$  = pullout load at pullout angle of  $0^\circ$  (N),  $f$  = snubbing coefficient (0.4),  $\theta_f$  = pullout angle of fiber (rad),  $\sigma_{fu}$  = rupture strength of fiber (MPa),  $\sigma_{fu}^n$  = rupture strength at pullout angle of  $0^\circ$  (MPa),  $f'$  = strength reduction factor (0.3).

The effect of improvements in pullout resistance is not considered in cases of a pullout angle  $45^\circ$  or more, because reduction of maximum pullout loads is confirmed in the case of polypropylene (PP) fiber used in this study. This was caused by the matrix spalling at the fiber exit point as reported [6].

## 4 ANALYSIS OF FIBER PULLOUT BEHAVIOR IN ADVANCED MODEL

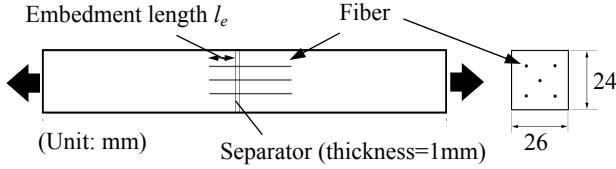
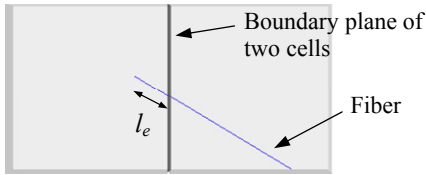
In this chapter, the pullout behavior of fibers embedded in the matrix is verified, through an analysis using the advanced model described in the previous chapter.

### 4.1 Pullout behavior of a single fiber

As shown in Figure 5, tensile analysis was conducted for a uniaxial tension test using

**Table 1:** Material properties for the analysis.

Fiber (PP)	Length $L_f$ (mm)	30
	Diameter $d_f$ (mm)	0.8
	Elastic modulus $E_f$ (GPa)	9.8
Fiber/concrete Interface (bond)	Frictional bond strength $\tau_i$ (MPa)	1.8
	Chemical bond strength $\tau_c$ (MPa)	4.0
	Bond stiffness $G$ (MPa/mm)	60


**Figure 5:** Outline of fiber pullout test (Dong et al.).

**Figure 6:** Analysis model.

specimens containing fibers [6]. While this test conducted by Dong et al. used a specimen containing five strings of fiber, this analysis applied the model embedded a single fiber, as shown in Figure 6. The entire body of the matrix is divided into two elements and the fiber is arranged, so that predetermined embedment length and pullout angle are given. In order to represent the separator in the test (Figure 5),  $1\text{N/mm}^2$  is used for the physical properties of the concrete elastic modulus, to prevent matrix from being loaded. Table 1 shows the characteristics of the short fiber and fiber-concrete interface used for the analysis. The properties of the interface are identified by a similar method in an existing study [3].

Figure 7 shows the relationship between the bridging force per fiber and crack width in the case of pullout angle  $\theta_f = 0^\circ$ . Once the loads reach a peak, the fiber is found to be pulled out with a moderate reduction of loads. The value of displacement at complete pullout is 15mm. This value corresponds to embedment length  $l_e$ . As mentioned above, the results from this model are controlled by the pullout behavior

of shorter embedment length on each fiber.

The deformation and the fiber bridging force-crack width curves in the case of  $\theta_f > 0^\circ$  are as shown in Figures 8 and 9, respectively. In the case of  $\theta_f = 75^\circ$ , the initial stiffness is smaller in the experimental results than the analytical results. This is assumed to be because a deceptive pullout displacement increased by the matrix spalling at the exit point in the experiments, once the angle becomes  $\theta_f > 45^\circ$ , as reported [6]. The effect of this phenomenon is not considered in this modeling. As a result, the initial stiffness of the fiber bridging force-crack width curves in the case of  $\theta_f > 45^\circ$  is overestimated.

## 4.2 Pullout behavior of a single fiber under mode II fracture

An analysis was conducted in order to study pullout behavior of the fiber under mode II fracture using the same model as that described in the previous section. Forced displacement is given to reach mode II fracture in this analysis.

Figures 10 and 11 show the fiber bridging force-shear displacement curves and the deformation, respectively. The conventional model would not resist fiber bridging force under mode II fracture in order to assume the fiber pullout displacement to be the crack width, as aforementioned. With this advanced model, the fiber is found to resist the bridging force. Note that there are few test reports of such tests verifying a pullout behavior at an angle of  $\theta_f > 90^\circ$  in previous studies, so that data should be further collected to verify this model.

## 4.3 Pullout behavior of multiple fibers

The authors conducted uniaxial tensile analysis and shear analysis to verify the fiber pullout behaviors of a specimen containing multiple fibers.

Figure 12 shows the analysis model. The fibers are placed in the specimen using random numbers. The fiber volume fraction  $V_f$  is 2%. The fibers shown in Table 1 are used in the

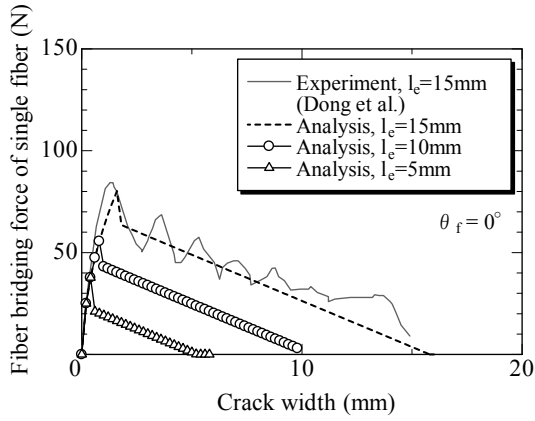


Figure 7: Fiber bridging force-crack width curves ( $\theta_f = 0^\circ$ ).

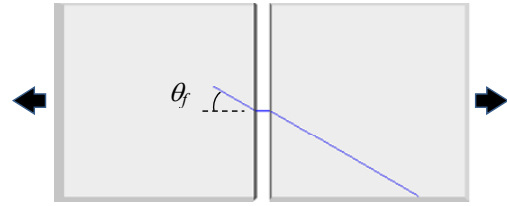


Figure 8: Deformation in tensile analysis (mode I).

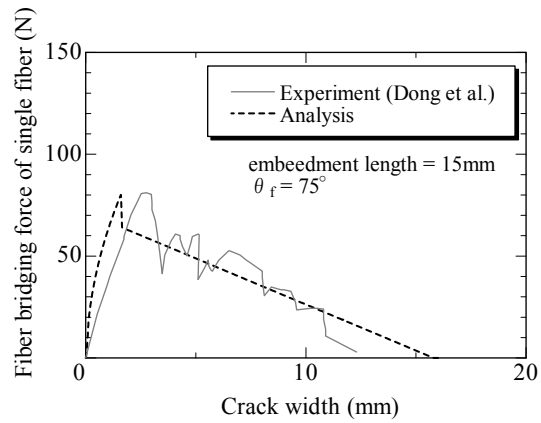
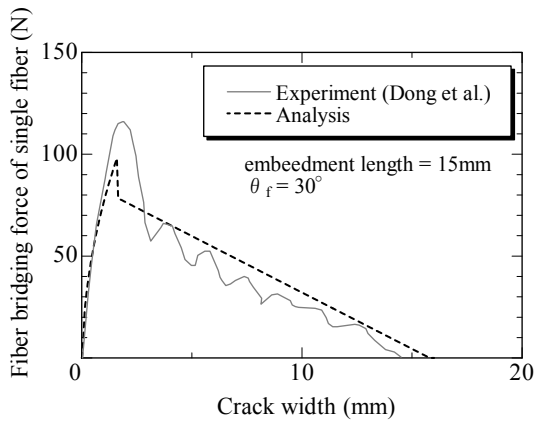


Figure 9: Fiber bridging force-crack width curves ( $\theta_f > 0^\circ$ ).

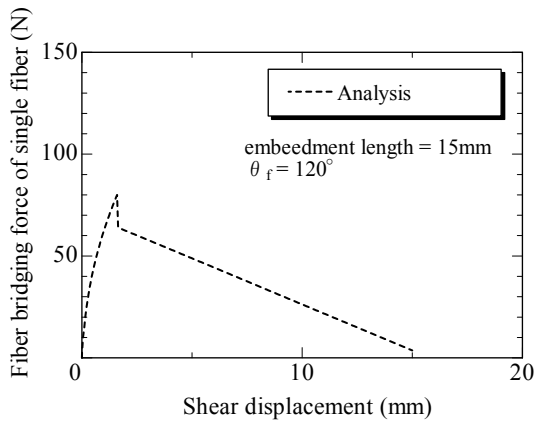


Figure 10: Fiber bridging force-shear displacement curves.

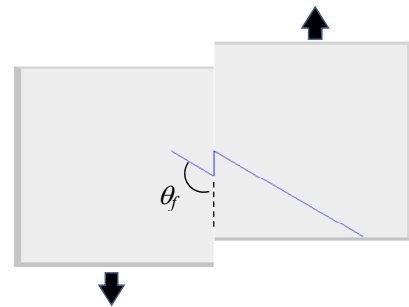


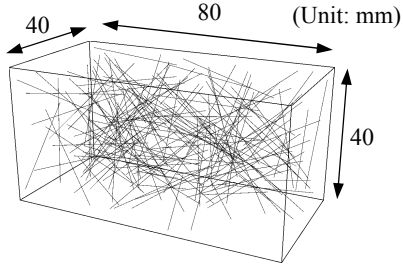
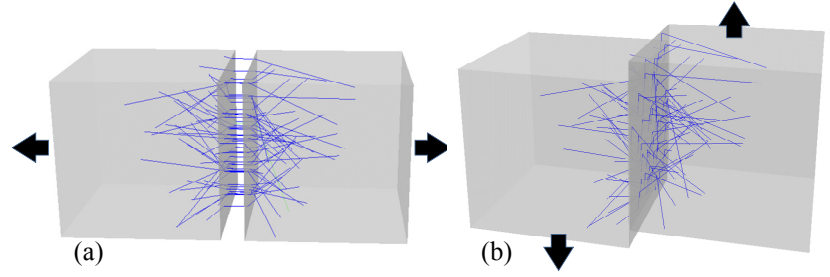
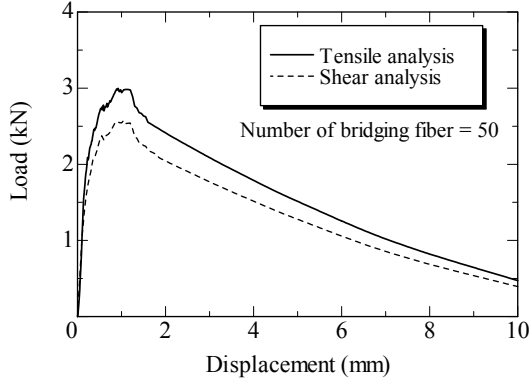
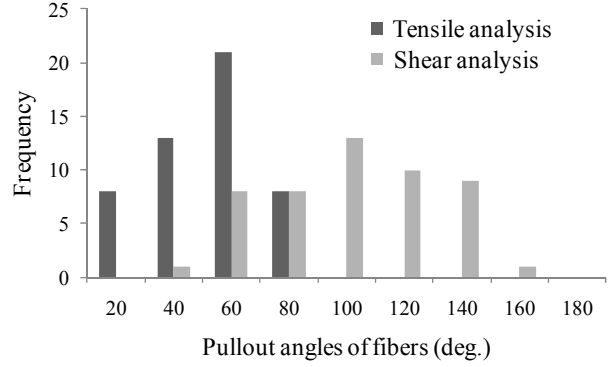
Figure 11: Deformation in shear analysis (mode II).

same as the analysis in the previous section.  $1\text{N/mm}^2$  is used for the physical properties of the concrete elastic modulus, so that it would not resist stress.

The deformation results taken from the analysis and the load-displacement curves are shown in Figures 13 and 14, respectively. Once the load reaches a peak, the fibers are found to be pulled out with moderate reduction of loads, from the results of both tensile

analysis and shear analysis.

Figure 15 shows the frequency distribution of pullout angles of fibers. In the tensile analysis, the fibers are pulled out in vertical directions against cracks. Therefore, the pullout angle  $\theta_f$  is less than  $90^\circ$ , as shown in Figure 15. On the other hand, the result showed that the pullout angle of the shear analysis is distributed from acute angles to obtuse angles.


**Figure 12:** Discretized fibers.

**Figure 13:** Deformation: (a) Tensile analysis; (b) Shear analysis.

**Figure 14:** Load-displacement curves.

**Figure 15:** Frequency distribution of pullout angles of fibers.

## 5 VALIDATION OF ADVANCED MODEL

In this chapter, analysis is conducted on punching shear tests to validate the advanced model.

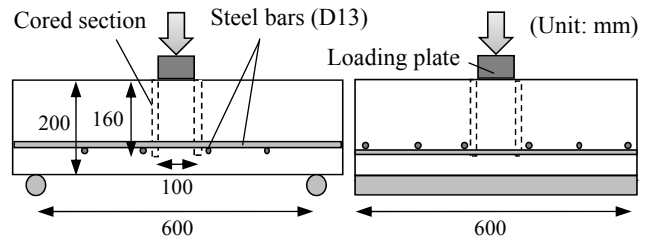
### 5.1 Outline of punching shear analysis

Figure 16 shows the overview of the punching shear test. This test was conducted to evaluate the resistance against falling of concrete pieces, conducted by Nojima et al. [8], according to the standards of Japan Society of Civil Engineers. The specimen center was cored with a margin of 40mm, and conducting a punching shear test. It simulates falling of concrete pieces caused by reinforcement corrosion. Volume fraction of fiber was 0.71% and PP fibers were used as shown in Table 2.

The analysis model is shown in Figure 17. The cored section of the specimen is also modeled. Short fibers of the specified length are randomly arranged in the elements assuming the specimen size. Steel bars are modeled as a series of beam elements, which are connected to concrete through a link element [5].

As for the boundary conditions, forced vertical displacement is given to the elements located in loading plate.

The material properties of concrete for the analysis are given as elastic modulus 31.0kN/mm<sup>2</sup> based on the results of the material test. The properties of the fibers used for the analysis are as shown in Table 2. The properties of the interface between fibers and concrete are identical to Table 1 in the previ-


**Figure 16:** Overview of the punching shear test.

**Table 2:** Material properties for the analysis.

Fiber (PP)	Length $L_f$ (mm)	30
	Diameter $d_f$ (mm)	1.0
	Elastic modulus $E_f$ (GPa)	9.8
	Strength at pullout angle of 0° $\sigma_{fu}^n$ (MPa)	350

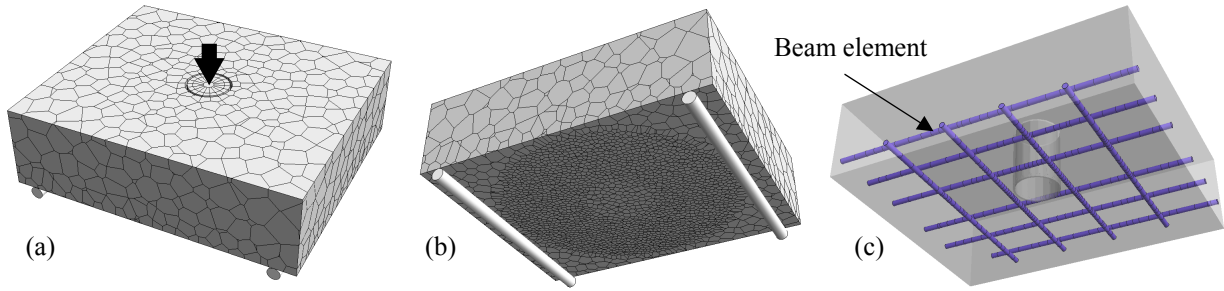
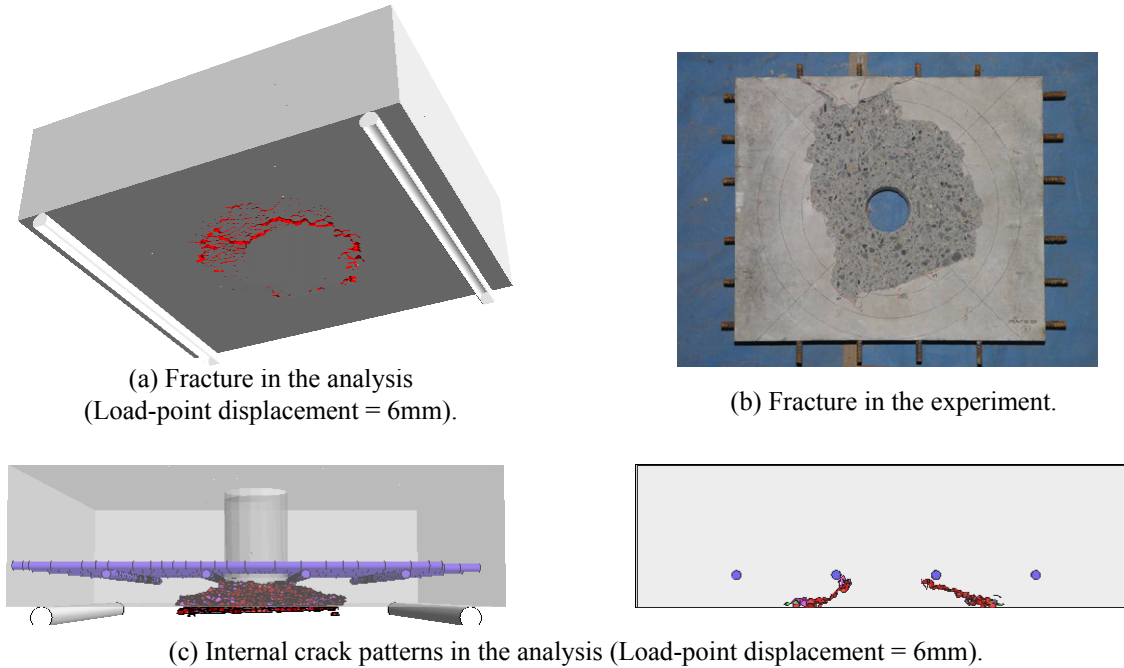


**Figure 17:** Modeling of punching shear test: (a) view from top; (b) view from bottom; (c) steel bars model.



(a) Fracture in the analysis  
(Load-point displacement = 6mm).

(b) Fracture in the experiment.

(c) Internal crack patterns in the analysis (Load-point displacement = 6mm).

**Figure 18:** Crack patterns.

ous chapter. The rupture strength at a pullout angle  $0^\circ$  is 70% of the nominal value, as confirmed in the previous tests that the value should be less than the nominal value disclosed by the manufacturer [7]. Note that the rupture strength varies depending on the pullout angle, as shown in Equation 2.

## 5.2 Results of analysis

Figures 18 and 19 show the results of the analysis, as well as experimental results. The analysis shows reinforcing effects of fibers are a little overestimated for the post-peak period, but the trend of the experiments is demonstrated. Crack patterns are found to be similar to the area of delamination observed in the experiment, as shown in Figure 18(b).

Figure 20 shows the relative frequency dis-

tribution of pullout angles of fibers. The analysis shows a wide distribution even for the obtuse angle. This suggests shear deformation across the crack plane occurs in punching shear analysis.

From the results of the experiment and analysis, the new analysis method using the advanced model is verified to be sufficient to reinforcing effects of fibers, even though there is significant shear deformation across the crack plane.

## 6 CONCLUSION

This paper has introduced the meso-scale modeling for fiber reinforced concrete under mixed mode fracture. The findings obtained include the following:

- (1) By analysis conducted on punching shear tests of fiber reinforced concrete, this

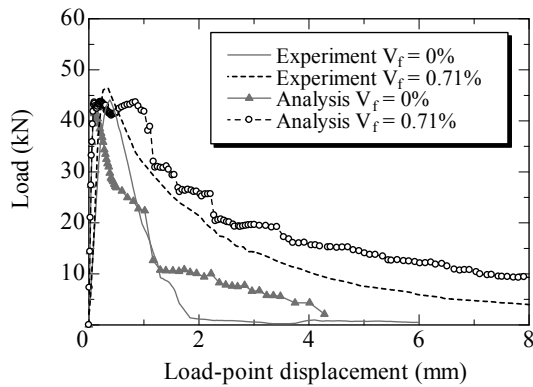


**Figure 19:** Load-displacement curves.

model roughly simulated mechanical response represented by load-displacement relations and crack pattern under mixed mode fracture.

- (2) The modeling of pullout resistance against shear deformation along crack plane was essential to represent punching shear tests.

#### ACKNOWLEDGEMENT

The data of the punching shear tests were provided by Mr. Shoji Nojima, Nippon Expressway Research Institute Company Limited in the conduct of this study. The authors would like to acknowledge this support.

#### REFERENCES

- [1] Bolander, J.E. and Saito, S., 1997. Discrete modeling of short-fiber reinforcement in cementitious composites. *Advanced Cement Based Materials*, Vol. 6, pp. 76-86.
- [2] Kunieda, M., Ogura, H., Ueda, N. and Nakamura, H., 2011. Tensile fracture process of Strain Hardening Cementitious Composites by means of three-dimensional meso-scale analysis. *Cement & Concrete Composites*, Vol. 33, pp. 956-965.
- [3] Ogura, H. and Kunieda, M., 2009. Analysis for flexural failure behavior of PET fiber reinforced cementitious composites by means of 3-D meso-scale analysis. *Proc.*

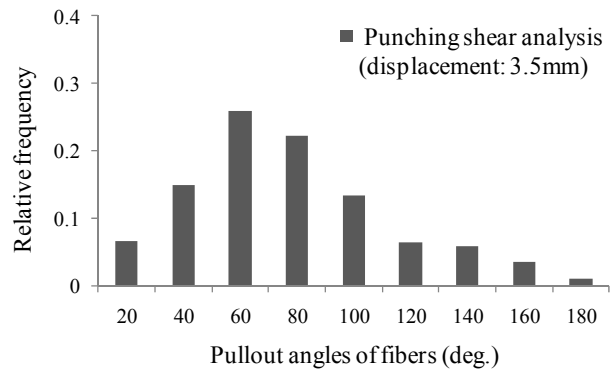


**Figure 20:** Relative frequency distribution of pullout angles of fibers.

of 33rd IABSE Symposium, pp. 272-273, CD-ROM(full paper).

- [4] Bolander, J.E. and Berton, S., 2004. Cohesive zone modeling of fracture in irregular lattices. *Fracture Mechanics of Concrete Structures, Proc. of FraMCoS-5*, pp. 989-994.
- [5] Saito, S., 1999. Fracture analyses of structural concrete using spring network with random geometry. *Doctoral thesis, Kyushu University*
- [6] Dong, H., Okubo, S. and Fukui, K., 2010. The bond characteristics with concrete and the effects of embedding angle and length of polyolefin fibers. *Journal of MMIJ*, Vol. 126, pp. 654-659. (in Japanese).
- [7] Kanda, T. and Li, V. C., 1998. Interface property and apparent strength of high-strength hydrophilic fiber in cement matrix. *Journal of Materials in Civil Engineering, ASCE*, Vol. 10, No. 1, pp. 5-13.
- [8] Nojima, S., Asai, T. and Ochiai, M, 2011. Methods of prevention for falling concrete pieces using fiber reinforced concrete. *Proceedings of the Concrete Structure Scenarios, JSMS*, Vol. 11, pp. 1-6. (in Japanese).